# Metastability effects on the photoluminescence of ZnO nano-micro structures grown at low temperature and influence of the precursors on their morphology and structure

# Metastability effects on the photoluminescence of ZnO nano-micro structures grown at low temperature and influence of the precursors on their morphology and structure

Vanessa González[1,2], Oscar Marin[1,3,£], Mónica Tirado[1,2] and David Comedi[1,3,*]

1. Instituto de Física del Noroeste Argentino (INFINOA), Consejo Nacional de Investigaciones Científicas y Técnicas (CONICET), Universidad Nacional de Tucumán (UNT), Av. Independencia 1800, San Miguel de Tucumán, 4000, Argentina.
2. NanoProject - Laboratorio de Nanomateriales y Propiedades Dieléctricas (LNPD), Facultad de Ciencias Exactas y Tecnología (FACET), Universidad Nacional de Tucumán (UNT), Avenida Independencia 1800, San Miguel de Tucumán, 4000, Argentina.
3. NanoProject - Laboratorio de Física del Sólido (LAFISO), Facultad de Ciencias Exactas y Tecnología (FACET), Universidad Nacional de Tucumán (UNT), Avenida Independencia 1800, San Miguel de Tucumán, 4000, Argentina.

£ Corresponding author: omarin@herrera.unt.edu.ar
*Corresponding author: dcomedi@herrera.unt.edu.ar

## Abstract

Nanocrystalline ZnO films were grown on silicon substrate by hydrothermal synthesis at 125 °C, using diethanolamine as additive. A powder containing ZnO spheres, with diameters between 100 to 200 nm and formed by aggregation of ZnO nanoparticles, was also obtained as a secondary reaction product. The samples were studied by scanning electron microscopy, X-ray diffraction and photoluminescence (PL) spectroscopy. The effects of the [diethanolamine]/[$Zn^{2+}$] molar ratio on morphological, structural and optical properties were studied, as well as the effect of laser illumination ($\lambda$=325 nm) and annealing treatment on photoluminescence properties. The film samples exhibited a compact columnar structure, with thickness between 180 to 210 nm, which were not strongly affected by the diethanolamine concentration. The X-ray diffraction patterns from the films evidenced preferred orientation along the c-axis of the ZnO wurzite structure; while the nanospheres did not show any preferential crystalline direction. The PL spectra from the films showed large initial UV emission and a weak defect band centered in the yellow. A PL evolution while the samples were UV illuminated was observed. The relaxation of metastable phases (formed during the low temperature growth) involving the creation of point defects, is suggested. The predominance of the

yellow defect band before and after treatment points at oxygen vacancies as the possible point-defect candidate.

***Keywords:*** *ZnO thin films; Hydrothermal synthesis; Photoluminescence; Metastability effects; Diethanolamine; Oxygen vacancies; ZnO nanospheres.*

## 1. Introduction

Nano and microsized wide bandgap semiconductors exhibiting different morphologies, such as nanostructured films, nanowires, nanoparticles, nanobelts, microspheres and others, have important technological interest in many areas, such as electronic, optoelectronic and photovoltaic applications [1,2]. Among this type of materials, ZnO has been extensively studied due to its bandgap in the UV (3.37 eV at room temperature), large exciton binding energy (60 meV) [3,4] and an interesting combination of electronic and optical properties that make it suitable for electronic, photovoltaics, UV LEDs and UV photodetector applications [5–8]. Some of these properties can be tuned by varying the structure morphology (particle size, aspect ratio, surface area, shape, which depends on the growth methods and synthesis conditions [9,10].

Different nanostructured materials have been obtained through a large variety of techniques that allow the control and systematic manipulation of their properties. Within these, colloidal routes such as the hydrothermal synthesis, chemical bath deposition and the sol-gel technique, stand out due to several advantages, including low or intermediate synthesis temperatures and excellent control of the fabricated material properties [11–14].

In particular, the hydrothermal route allows ZnO synthesis at lower temperatures than those used in sol-gel (wide range of temperature) [15] and much lower than used in other techniques, such as chemical vapor deposition or vapor transport with carbothermal reduction (> 950 °C) [3,12,16]. These advantages and the fact that it is a rapid technique that can produce high quality product with high yields at low costs make the hydrothermal synthesis method a very promising candidate for future industrial applications.

Several ZnO morphologies have been reported using hydrothermal synthesis, especially nanowires. Growth parameters such as temperature, pressure, pH and additives (capping, chelating or stabilizing agents) affect the characteristics of the obtained product; however, the growth mechanisms are not completely known [17].

Within the parameters mentioned, the additives play a crucial role, not only because they control the pH of the reaction medium or the formation of a stable colloidal phase, but also because they act as crystal growth modifiers through the change of the growth kinetics for specific crystalline faces [18], which determine different morphologies. One of the additives frequently used in hydrothermal synthesis is diethanolamine (DEA), which acts as an alkaline source [19]. However, the influence of the [diethanolamine]/[$Zn^{2+}$] molar ratio on the morphological and structural properties of ZnO obtained through hydrothermal synthesis has not yet been studied in depth.

Nonetheless, since the growth is carried out at low temperature, a key factor to keep in mind with hydrothermal routes is the possible presence of amorphous/metastable phases or its coexistence with crystalline phases [20,21], in a similar way to the reported for some sol-gel derived ZnO films [22,23]. This behavior can be understood by considering that the crystallization process implies transitions between different metastable phases until the most stable state is reached [21]. Hence, the low atomic mobilities and other kinetic limitations associated with the low temperature used in the synthesis may lead to an incompletely crystallized atomic network at the end of the growth process [20]. Hence, it is expected that there will be a slow relaxation of metastable states present in the as-grown material, which may lead to changes in the optical properties. Such a relaxation can be accelerated by introducing energy to the system. For example, for sol-gel synthetized ZnO films, structural changes induced by UV irradiation that resulted in changes in the film's transmittance have been reported [22,23]. Since the relaxation of metastable phases occurs through atomic scale rearrangements, formation or annihilation of point defects is expected during this process, leading to changes in photoluminescence spectra. UV irradiation induced evolution of photoluminescence in different materials, such as porous silicon [24], polypyrrole [25] and $TiO_2$ [26], has been reported. For ZnO, the evolution of the photoluminescence caused by UV irradiation has been reported to occur at cryogenic temperatures [27].

In this work, we report on the use of DEA as an additive agent and study the role of the DEA concentrations on the formation of ZnO thin films on silicon substrates. As a secondary reaction product, a white precipitate powder composed by spheres with sizes on the order of hundreds of nanometers is obtained. The fact that this synthesis routine leads to two separated, distinct types of products represents an interesting

industrial potentiality, not only for its double outcome but also for the full exploitation of reactants. The samples were studied by x-ray diffraction (XRD), scanning electronic microscopy (SEM) and photoluminescence spectroscopy (PL). Since point defects present in the ZnO lattice (oxygen and zinc vacancies, interstitial zinc and others) act as radiative recombination centers, the PL technique provides a useful overall diagnosis of the nature of such defects [11]. The films obtained initially exhibited high UV emissions, weak defect emissions in the yellow, and preferential orientation along the c-axis of wurtzite. However, photoinduced effects were evidenced by the evolution of PL spectra at room temperature while samples were UV illuminated. A decrease in the UV emission is accompanied by an increase of the defect emission. We propose the relaxation of metastable phases (formed during the low temperature growth) involving the creation of point defects as the origin of these changes; the PL spectra of the annealed samples strengthen this hypothesis.

## 2. Experimental details

### 2.1 Sample preparation

First, (1 0 0) oriented silicon substrates of ~1cm×1cm size were cleaned by immersion in ethanol and acetone with ultrasonication. Then, ZnO seeds were deposited on the Si substrates using an ethanolic solution of zinc acetate dihydrate [$Zn(CH_3COO)_2{\cdot}2H_2O$, Sigma Aldrich] 20 mM. For this purpose, 100 μL of this ethanolic solution was dropped on the silicon substrate and spinned at 1500 rpm during 1 min, then, it was dried at 125 °C for 5 min. This procedure was repeated 6 times; finally, the substrates were heated during 4 h at 125 °C to improve the adherence of the seeds.

Samples were synthesized with different [DEA]/[$Zn^{2+}$] molar ratios ($X_{DZ}$), using distilled water, DEA (Ziccarelli) and zinc acetate dihydrate as the $Zn^{2+}$ precursor (50 mM, aqueous solution) in a 25 mL stainless steel autoclave with Polytetrafluoroethylene (PTFE) vessels. The silicon substrates with the ZnO seeds were immersed upside down in a vertical inclined position into the PTFE vessels, which contained, added in this order, 1.5 mL $Zn^{2+}$ precursor solution, DEA in the required quantities to obtain mixtures with $X_{DZ}$ =14, 28, 42, 56 or 70 and water (until completing 12.5 mL, i.e 50% of autoclaves capacity). Then, the autoclaves were closed and heated for 4 h at 125 °C and, they were cooled down to room temperature. Finally, the samples were washed with water and dried at 125 °C in air for 1 h. Each one of the white precipitates formed were

washed with distilled water and redispersed in ethanol; the precipitates were drop casted on silicon substrates and dried at 125 °C for ethanol evaporation.

### 2.2 Sample characterization

The sample morphology and particle sizes were studied by SEM using a Carl-Zeiss model Supra 55-VP and a Zeiss Supra 40 field emission microscope. Mean grain sizes and sample thicknesses were determined by analyzing SEM images using ImageJ open source software. Surface grains were identified and their size measured on SEM images; mean sizes and corresponding standard deviations were calculated and then the output data were rounded up in consistency with the expected accuracy of the SEM instrument.

The crystalline structure of selected samples was studied by XRD using a SIEMENS D5000 diffractometer with Cu Kα radiation source (1.54056 Å). The patterns were recorded in the 30-80° diffraction angle range. PL spectra were recorded using a backscattering geometry with a He-Cd laser set at a wavelength of 325 nm (15 mW) as the excitation source; the light emitted by the sample was focalized on a CCD spectrometer with two biconvex lenses. A filter was placed at the entrance of the spectrometer to eliminate scattered laser radiation.

## 3. Results

### 3.1 Morphology and crystalline structure

As a consequence of the hydrothermal synthesis reaction, two different products were obtained: (i) a thin film grown on the silicon substrate and (ii) a white precipitate powder. In Figures 1a-d, SEM micrographs of the ZnO thin films for the different $X_{DZ}$ are shown. The films obtained exhibit a compact nanocrystalline structure showing an increment of grain size from ~ 49 nm for $X_{DZ}$ = 28 to ~ 100 nm for the highest $X_{DZ}$ value; these results are summarized in Table 1. High thickness uniformity is evidenced by the cross-sectional views shown in Figures 1(e-i). In addition, these micrographs reveal the formation of a double layer structure, which is more evident in the films grown using $X_{DZ}$ values of 28 and 70. As it is observed, the bottom layer is composed by particles in the nanoscale and the top layer follows a columnar-type growth.

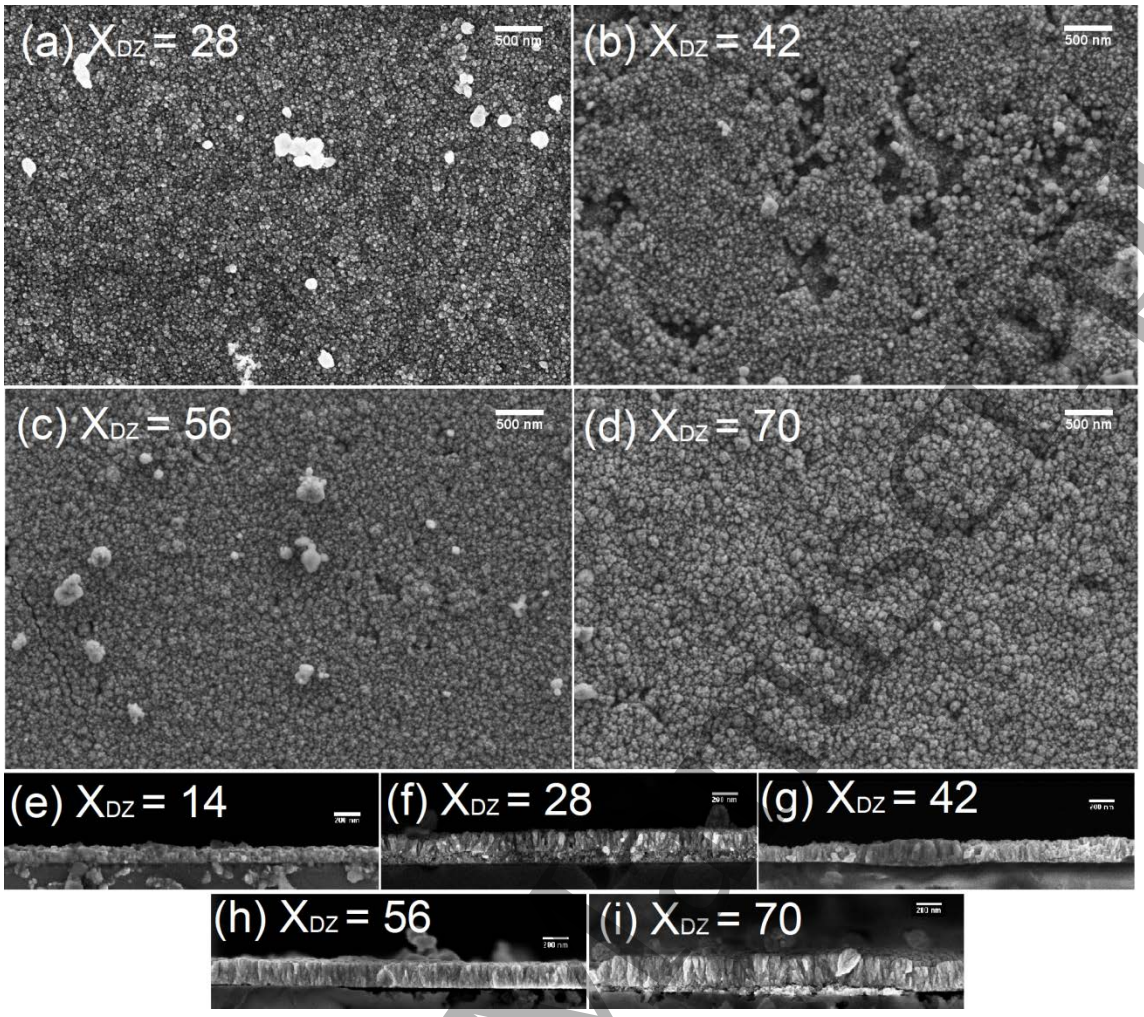


Fig. 1 SEM micrographs of ZnO thin films grown varying $X_{DZ}$. (a-d) top view, the scale bar is of 500 nm; (e-i) cross-sectional view, the scale bar is of 200 nm.

In Fig. 2 the SEM micrographs corresponding to samples extracted from the white precipitated powder (second product of hydrothermal synthesis) and casted on silicon sustrates are shown. These images reveal that the powders are composed of quasi-spherical particles with diameters in the range of hundreds of nanometers, but with a large size dispersion. The average particle sizes for the different samples are plotted as a function of $X_{DZ}$ in Fig. 2(f), with bars indicating the corresponding standard deviations. It is clear that the variation of $X_{DZ}$ does not significantly affect the average particle size. In addition, observations at higher magnification (insets of Figures 2a-e) reveal that these particles have a structure in the nanoscale. Apparently, they areaggregates of many ZnO nanoparticles, as has been previously reported for solvothermal synthesis [28,29]. However, in our case, when $X_{DZ}$ is increased, their surfaces become smoother (see insets in Figures 2a-e).

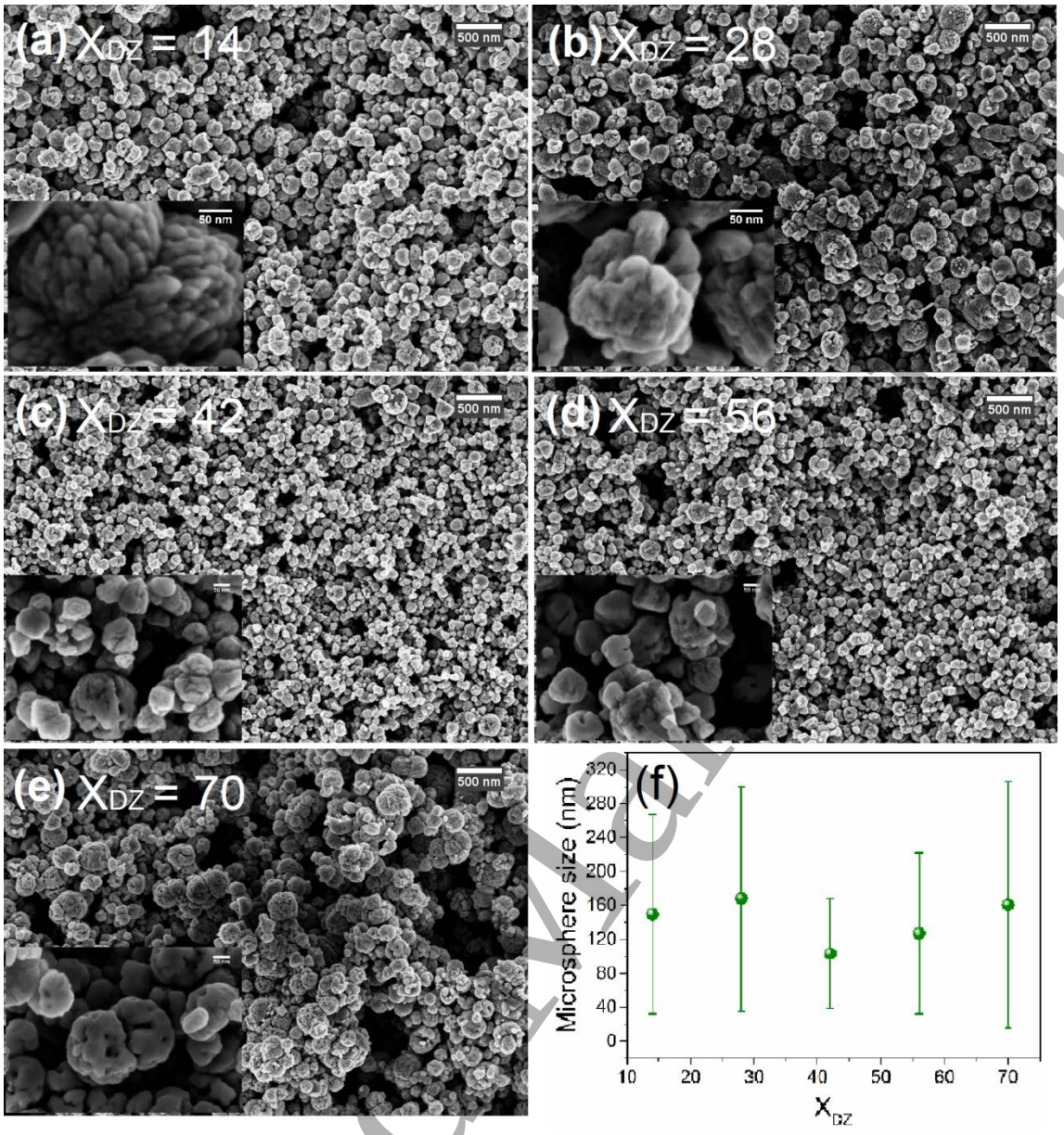


Fig. 2 SEM micrographs of ZnO white precipitated powder with different $X_{DZ}$, a) $X_{DZ}$ = 14, b) $X_{DZ}$ = 28, c) $X_{DZ}$ = 42, d) $X_{DZ}$ = 56, e) $X_{DZ}$ = 70. The images were taken with 50 KX of magnification, the scale bar is of 500 nm. (f) Microsphere size obtained from SEM micrographs.

The sizes of the particles that grew within the precursor solution are lower that the reported values for microparticles synthetized by solvothermal technique using ethanolamine family as the additive agent [28–30]. For the specific case of synthesis at 150°C using a one-to-one ethanolamine to [$Zn^{2+}$] molar ratio and ethanol as a solvent, a size of 3-4 μm was reported [29].

*Table I. Film thickness, mean film grain size and mean submicrosphere diameter for various ZnO products obtained from hydrothermal synthesis experiments for different $X_{DZ}$.*

| $X_{DZ}$ | Film thickness (nm) | Mean film grain size and standard deviation (nm) | Mean submicrosphere diameter and standard deviation (nm) (μm) |
|---|---|---|---|
| 14 | - | - | 150 ± 120 |
| 28 | 230 | 50 ± 20 | 170 ± 130 |
| 42 | 170 | 60 ± 30 | 100 ± 60 |
| 56 | 180 | 80 ± 30 | 130 ± 100 |
| 70 | 230 | 100 ± 50 | 160 ± 150 |

In Fig. 3, the XRD patterns from the thin films obtained with $X_{DZ}$ = 14 and 70 and the submicrospheres obtained with $X_{DZ}$ = 56 and 70, are shown. In both cases, the XRD data are compared with a pattern from a standard ZnO polycrystalline powder sample (in black). As it is evident, the thin films grew with a polycrystalline structure with preferential orientation normal to the (002) plane, corresponding to the c-axis of wurtzite. Secondary peaks, corresponding to (101) and (102) planes, are also observed; however the (002) and (101) diffraction peaks are broad and overlap into a merged peak, whose intensity increases (suggesting increased crystallinity) with increasing $X_{DZ}$. In contrast, the submicrospheres do not show any texture and their patterns are similar to that from the ZnO standard sample.

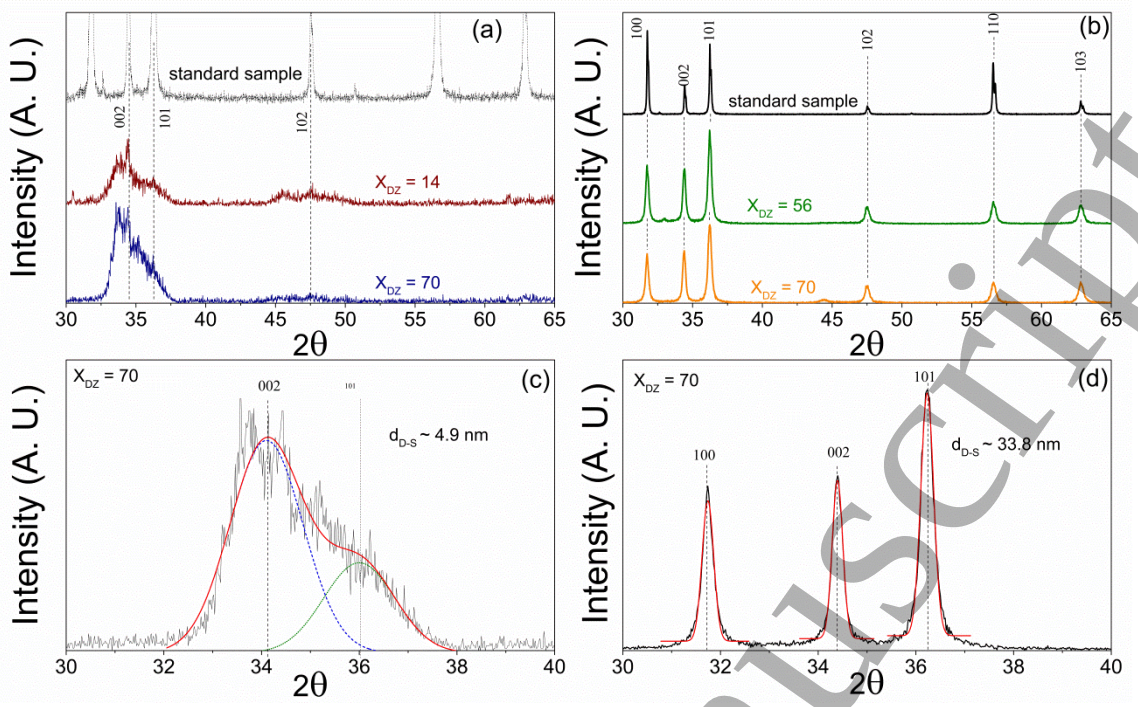


Fig. 3 X-ray diffraction patterns for selected samples, a) films with $X_{DZ}$ = 14 and 70, b) submicrospheres powder with $X_{DZ}$ = 56 and 70. In both cases, the XRD data are compared with a pattern from a standard polycrystalline ZnO sample (in black).

Two kinds of effects could contribute to the diffraction peak broadening, i.e those due to i) crystallite size , and ii) lattice strain [31]. The relation of crystallite size and the peak broadening can be estimated with the well-known Scherrer's equation: $D = K\lambda/\beta Cos\theta$, where $D$ is the crystallite size, $K$ is a shape factor (~0.9), $\lambda$ is the X-ray wavelength, $\beta$ is the diffraction peak FWHM and $\theta$ is the Bragg angle [14]. Assuming crystallite size effects only, one would obtain D ~5 nm for the ZnO films and D ~ 35 nm for the submicrospheres. Furthermore, for a crystallite size of ~5 nm, a relatively large blueshift of the UV emission band in the PL spectra would be expected [4], placing the band maximum in the 365-369 nm range [32,33]. As shown in the next subsection, the UV PL band maximum wavelength position is 376 nm.

Taking the above into account, we believe the broadening and the overlapping of the diffraction peaks from the films occur mainly due to the presence of non-uniform strain that could result from both compressive and tensile stresses in different regions [34,35]. Since the diffraction patterns for the films are noisy, it is not possible to refine the data accurately under the pattern matching mode of FullProf software. However, there apparently exist contributions from both the (002) and the (101) crystalline planes, which may indicate that the strain appears not only along the perpendicular direction to the substrate, but also along parallel directions. It is possible that the origin of the non-

uniform strain in these films stems from the double layer formation observed in the cross section SEM images in Figures 1e-i.

In the case of the submicrospheres, the lattice parameters were found using the FullProf software in the pattern matching mode (Le Bail refinement) [36]. For the sample synthetized with $X_{DZ}$ = 56, the *a* and *c* parameters values were 3.2533 and 5.2129 Å, respectively, which are slightly shorter than the corresponding values determined for the sample synthetized with $X_{DZ}$ = 70 (3.2543 and 5.2137 Å). In addition, the lattice parameters for both analyzed samples were longer than the values typically reported in the literature for ZnO (3.2475 – 3.2501 Å and 5.2038 - 5.2075 Å, respectively [37,38]).

**3.2 Photoluminescence**

The optical properties of the ZnO samples were studied by PL spectroscopy. The spectra show a peak in the UV due to near-edge excitonic transitions with maximum at 376 nm , and a broad band in the visible (centered at ~570 nm) due to transitions involving defect states within the bandgap. However, the spectra were observed to evolve while the samples were continuously excited with the laser radiation (3.81 eV). This is shown in Fig. 4; while the emission band in the visible increased, the UV emission decreased.

In Fig. 5, both the UV and the visible integrated intensities are shown as functions of the excitation time. It is clearly seen that the UV emission reaches a saturation value in a shorter period of time than the visible emission for low $X_{DZ}$; for $X_{DZ}$ = 28 and 42 the visible band intensity does not even reach saturation during the experiment.

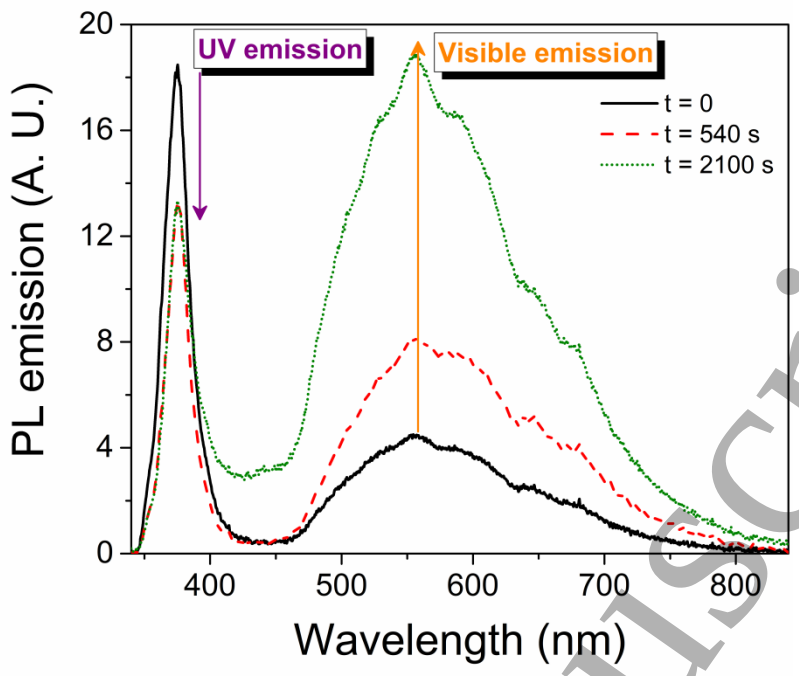


Fig. 4. Evolution of the photoluminescence spectrum as function of the excitation time for the sample grown with $X_{DZ}$ of 28. The legend indicates the excitation times at which each spectrum was acquired.

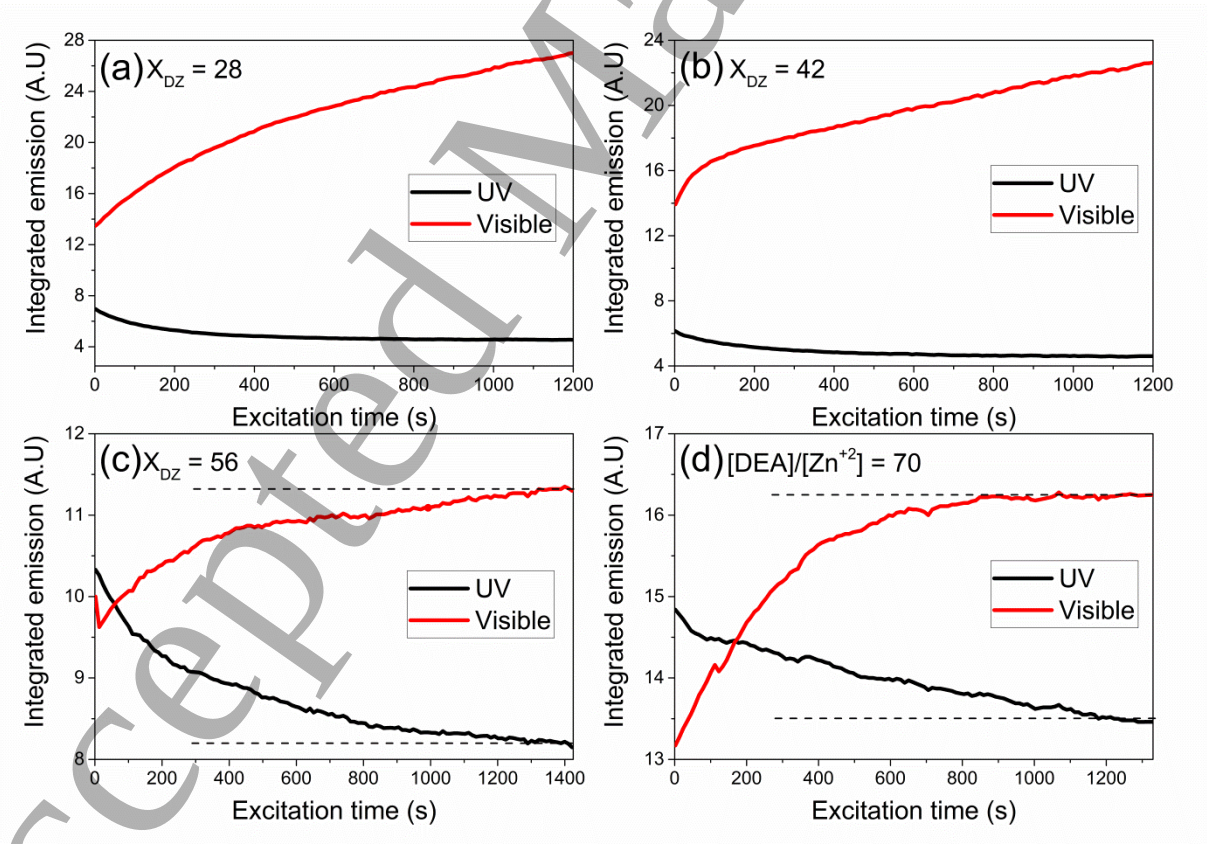


Fig. 5. Integrated UV and visible emission band intensities as functions of the excitation time.

It is interesting to note that the emission band in the visible is centered in the yellow (λ ~ 570 nm) at all excitation times. Similar emission in the yellow has been observed from ZnO samples grown by wet-chemical routes, in contrast to samples grown by physical routes, like vapor transport, where green band centered at λ ~ 530 nm is usually observed. In turn, the UV emission is peaked at ~376 nm (~3.30 eV). In order to compare PL spectra from different samples grown with different $X_{DZ}$, spectra were acquired with identical laser irradiation intensity during 1500 s each. The results are shown in Fig 6. Note that, while this excitation time is sufficient for the saturation of the UV band intensity from all samples, saturation of the visible emission is not achieved for $X_{DZ} \leq 42$. As clear from Fig. 6b, the UV emission increases with increasing $X_{DZ}$.

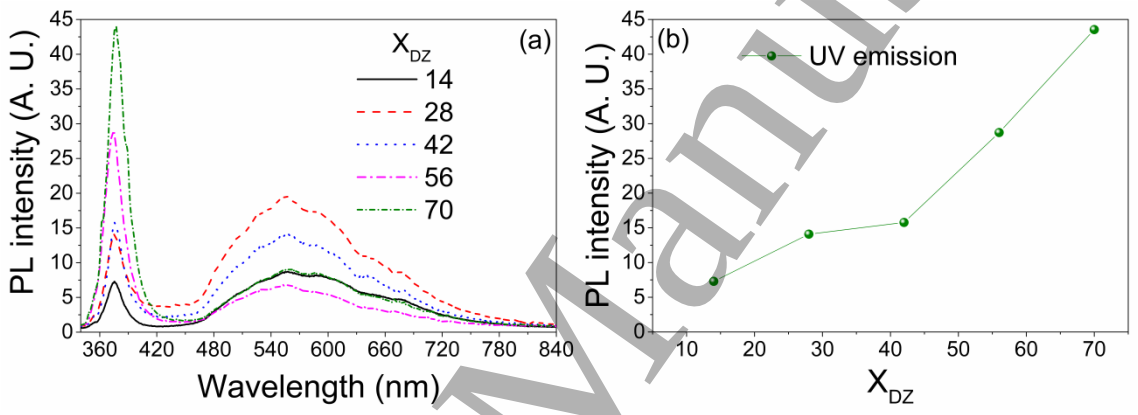


Fig. 6. (a) Photoluminescence spectra from films synthetized with different $X_{DZ}$, and (b) saturation integrated UV PL intensity as a function of $X_{DZ}$.

**4. Discussion**

DEA molecules combine the properties of amines, which act as weak base and alcohol, with two hydroxyl groups. Therefore, DEA is able to carry out reactions common to both groups. To properly understand and explain this synthesis process, it is reasonable to consider the crystal growth phenomena within two zones: i) a near substrate region where heterogeneous growth processes occur and the film growth is controlled, and ii) a zone away from the substrate, where homogeneous growth processes occur and the formation of submicrospheres is observed. Both the ZnO film and the submicrospheres growths involve complex and multiple stages; the DEA fulfills multiple functions during the ZnO synthesis by hydrothermal routes, including presumably:

i) Reaction stabilization through the formation of a stable colloidal media by the chelation of $Zn^{2+}$ ions (via amine-Zn ligand) and the polymerization of DEA – Zn – O

– Zn – DEA chains (in a similar way to sol formation in the sol-gel growth technique [14,39]).

ii) Providing a growth medium at basic pH to ensure the formation of metastable species that act as intermediate ZnO precursors, as is the case of zinc hydroxides.

iii) Morphology control by coordinating and modifying the growth rates of specific crystallographic faces. Indeed, for additives from the ethanolamine family, as is the case of DEA, the inhibition of the growth along the c-axis has been reported, explaining why large aspect ratio nanostructures such as ZnO nanowires are not obtained for this reagent family, with the spherical shape being the preferred morphology [30,40].

iv) Nanoparticle agglomeration facilitation. In a first stage, ZnO nanoparticles are formed and their morphology is defined by the surface coordinated DEA (point iii); these DEA molecules can act as bridges between nanoparticles, agglomerating them and consequently forming the observed submicrospheres [29,40].

Due to the fact that no significant thickness variation was observed between the obtained samples (see Table I), it is reasonable to assume that, at least in the range of $X_{DZ}$ values studied in this work, the DEA concentration does not affect the axial film growth rate (i.e. in the c-axis direction), but it does affect the transversal growth rate, as indicated by the grain diameter increase observed by SEM (Table I). In the spherical particles case, the role of DEA as an agglomerating agent of nanoparticles is evident, at least for the low $X_{DZ}$ values; for higher values its contribution does not seem so clear. For the case of film growth, the DEA does have a nanoparticle agglomeration agent role only in the first stages, as indicated by the growth of a nanoparticulate layer (Figures 1e-i). Nevertheless, after few nanometers growth, a compact columnar film is formed, thus indicating that the role of DEA changes at late stages. It is also clear from the crystallographic orientations deduced from the XRD experiments that the formation mechanisms for films and submicrospheres are different.

Taking into consideration the high DEA concentrations ($X_{DZ} >> 1$) used in our experiments, we believe the dominant roles of DEA during growth of our samples are i) and ii) (i.e. reaction stabilization and providing a basic medium that favor Zn hydroxide formation as an intermediate Zn precursor). In our experiments, the $X_{DZ}$ value was increased by keeping the Zn acetate concentration constant while increasing the DEA concentration. Although more studies would be needed to determine the film growth mechanism, it is clear that the growth rate (~ 0.7 nm/min, nearly constant with increasing $X_{DZ}$ ; see Table I) was mainly limited by the amount of Zn atoms in the

precursor solution (also constant) and that the Zn hydroxide concentration was saturated. The main effect of increasing the DEA concentration was to produce films with increasing grain size (Table I), which indicates that the DEA molecules had an influence on the lateral growth of the ZnO columns that occurred during the second stage of the growth. It is possible that the DEA acted as a nucleation inhibitor for the columnar growth by providing steric limitations. A reduced number of sites available for ZnO nucleation probably enabled the growth of the wider ZnO grains observed in the SEM images.

Regarding the photoluminescence spectra and their evolution with laser illumination, two possible mechanisms can be considered: i) desorption of molecular species bounded to the ZnO surface, ii) laser induced crystallization with the generation of point defects within the ZnO lattice. As to desorption of surface absorbed species (water, oxygen, hydroxyl species, among others), it has been reported that electron-beam irradiation and thermal treatment in air induce the desorption of water or hydroxyl groups from ZnO samples synthetized by wet chemical routes, improving UV emission [41,42]. Similarly, it has been reported that oxygen desorption enhances the UV emission in ZnO [43,44]. In our case, the reduction of the UV emission and increment of visible emission observed in Figure 6a allow us to rule out a mechanism related to desorption of surface species to explain the PL spectra evolution under laser radiation. On the other hand, taking into account that the visible emission is increased at the expense of the UV emission, it is probable that the dominant mechanism for PL evolution is related to the creation of point defects, basically because the electrons on the conduction band find new recombination channels (via additional luminescent point defects) while the competing near band edge recombination rate is reduced. Such formation of point defects could occur through the relaxation of metastable disordered crystalline phases present in the as-grown samples that result from the low atomic mobilities at the low temperatures involved in the hydrothermal growth process [22]. Indeed, the XRD patterns in Fig. 3 show that the as-grown films are poor in crystallinity while they exhibit relatively low defect PL (Figures 4, 5 and 6). This indicates that highly disordered metastable phases with relatively low point defect densities (i.e. lower than the equilibrium defect density) may have formed during the growth process. Hence, the equilibration of these metastable phases by annealing or illumination would lead to a more ordered structure and an increase in the point defect density. Even though it is not possible to state without a doubt the microscopic origin of the PL

evolution and the type of defects created, oxygen vacancies can be considered as possible candidates. This is mainly due to the fact that the visible emission is centered at the yellow, which has been associated with transitions involving oxygen vacancies [14,16]. In addition, the oxygen vacancy has lower formation energy than other point defects [45].

Since we have observed this effect occurring in samples fabricated by hydrothermal synthesis and not in ZnO samples grown by high temperature methods, we believe it is related to structural metastable configurations that result from the low temperature involved in the growth. To check the thermal stability of the effect, we carried out an annealing treatment of one of the samples ($X_{DZ}$ = 42) at 900 °C for 1 hour in air. Then, the sample was submitted to the regular UV excitation for the PL measurement. Fig. 7 shows the results together with those obtained for the unannealed reference sample. It is clear from Figures 7a-d (integrated UV and visible intensities as functions of the excitation time) that the annealing treatment leads to the stabilization of the PL spectrum under UV irradiation, since the PL intensities vary by less than 2% for the annealed sample as compared to ~30% variation for the as-grown (unnanealed) sample.

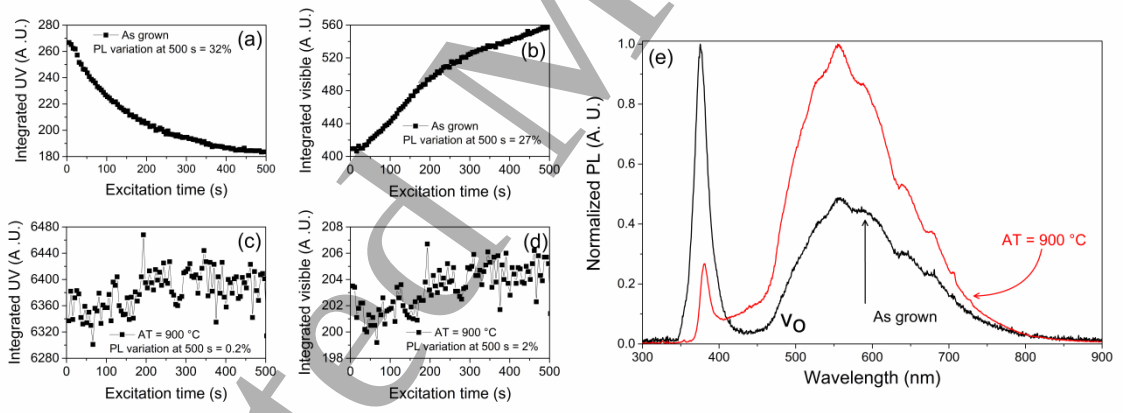


Fig 7. PL evolution of sample with $X_{DZ}$ = 42 after annealing at 900 °C in air. (a,b) integrated emission intensity from the as grown sample, (c,d) integrated emission intensity from the sample annealed at 900 °C for 1 h. (e) PL spectra for the as-grown (black) and annealed (red) samples.

In addition, as shown in Fig. 7e, the annealing treatment leads to a reduction of the UV emission intensity and an increase in the defect yellow band emission. The emission of this yellow band from the as-grown samples and its subsequent increase with annealing or laser illumination at the expense of the UV emission strongly suggest that the the ZnO film samples grown by the low-temperature hydrothermal synthesis are

in a metastable state characterized by a lower than equilibrium defect density, which increases towards its higher, equilibrium value by thermal annealing or by laser irradiation. Clearly, new experiments characterizing this metastability relaxation mechanism and kinetics, including the concomitant photoinduced creation of (probably vacancy) defects are called for.

## 5. Conclusions

ZnO thin films on Si substrates were fabricated through a sub-critical hydrothermal technique using DEA as additive. A powder formed by ZnO submicrospheres were obtained as a byproduct. The effect of varying the [DEA]/[$Zn^{2+}$] molar ratio ($X_{DZ}$) on the structural and optical properties of the thin films was studied. The following main conclusions can be drawn:

1) The thin films have a bilayer structure. A thin nanoparticulate layer grows first, which is followed by a thicker columnar structure.
2) A photoinduced change of the PL spectra from the ZnO films was observed. A decrease in the UV emission is accompanied by an increase of the defect emission induced by both, UV laser illumination and annealing treatment at 900ºC. The relaxation of metastable phases (formed during the low temperature growth) involving the creation of point defects, is suggested. The predominance of the yellow defect band before and after treatment points at oxygen vacancies as the possible point-defect candidate.
3) The high UV emission from these thin film samples positions them as excellent candidates for optical and optoelectronic devices; however their metastability and the stabilization of their emission characteristics need further studies.
4) The overall film thickness remains nearly constant, while its mean grain size increases, with increasing $X_{DZ}$. The XRD experiments evidence poor crystallinity with preferential growth direction along the c-axis of wurtzite. The observed peak broadening in the diffraction pattern gives evidence for the presence of non-uniform strain.
5) The ZnO powders composed by submicrospheres obtained as the synthesis byproduct exhibits a polycrystalline structure with no

preferential orientation. The average particle size does not change with the increase of $X_{DZ,}$ however, their surfaces become smoother.

**Acknowledgments**

We are grateful for financial funding by the National University of Tucumán (PIUNT 26/E535), and the Argentinean agencies CONICET (PIP 411) and ANPCyT (FONCyT – BID PICT 2015-0865).

**References**

[1] I. Matsui, Nanoparticles for electronic device applications: A brief review, J. Chem. Eng. Japan. 38 (2005) 535–546. doi:10.1252/jcej.38.535.

[2] X. Wu, P. Jiang, W. Cai, X.D. Bai, P. Gao, S.S. Xie, Hierarchical ZnO micro-/nano-structure film, Adv. Eng. Mater. 10 (2008) 476–481. doi:10.1002/adem.200700320.

[3] N.C. Vega, O. Marin, E. Tosi, G. Grinblat, E. Mosquera, M.S. Moreno, M. Tirado, D. Comedi, The shell effect on the room temperature photoluminescence from ZnO/MgO core/shell nanowires: Exciton-phonon coupling and strain, Nanotechnology. 28 (2017). doi:10.1088/1361-6528/aa7454.

[4] C. Sandoval, O. Marin, S. Real, D. Comedi, M. Tirado, Electrophoretic deposition of ZnO nanostructures: Au nanoclusters on Si substrates induce self-assembled nanowire growth, Mater. Sci. Eng. B Solid-State Mater. Adv. Technol. 187 (2014) 21–25. doi:10.1016/j.mseb.2014.04.002.

[5] H.D. Cho, A.S. Zakirov, S.U. Yuldashev, C.W. Ahn, Y.K. Yeo, T.W. Kang, Photovoltaic device on a single ZnO nanowire pn homojunction, Nanotechnology. 23 (2012). doi:10.1088/0957-4484/23/11/115401.

[6] R.L. Hoffman, B.J. Norris, J.F. Wager, ZnO-based transparent thin-film transistors, Appl. Phys. Lett. 82 (2003) 733–735. doi:10.1063/1.1542677.

[7] C. Tian, D. Jiang, B. Li, J. Lin, Y. Zhao, W. Yuan, J. Zhao, Q. Liang, S. Gao, J. Hou, J. Qin, Performance enhancement of ZnO UV photodetectors by surface plasmons, ACS Appl. Mater. Interfaces. 6 (2014) 2162–2166. doi:10.1021/am405292p.

[8] L. Zhang, Q. Li, L. Shang, F. Wang, C. Qu, F. Zhao, Improvement of UV electroluminescence of n- ZnO / p-GaN heterojunction LED by ZnS interlayer, Opt. Express. 21 (2013) 1613–1617. doi:10.1364/OE.21.016578.

[9] G. Grinblat, M.G. Capeluto, M. Tirado, A. V. Bragas, D. Comedi, Hierarchical ZnO nanostructures: Growth mechanisms and surface correlated photoluminescence, Appl. Phys. Lett. 100 (2012). doi:10.1063/1.4724195.

[10] S. Panigrahi, D. Basak, Morphology driven ultraviolet photosensitivity in ZnO-CdS composite, J. Colloid Interface Sci. 364 (2011) 10–17. doi:10.1016/j.jcis.2011.08.001.

[11] K.H. Tam, C.K. Cheung, Y.H. Leung, a B. Djuris, S. Fung, W.M. Kwok, W.K. Chan, D.L. Phillips, L. Ding, W.K. Ge, Defects in ZnO Nanorods Prepared by a Hydrothermal Method, J. Phys. Chem. B. 110 (2006) 20865–20871.

[12] L. Greene, B. Yuhas, M. Law, Solution-grown zinc oxide nanowires, Inorg. Chem. 45 (2006) 7535–43. doi:10.1021/ic0601900.

[13] R. Parize, J. Garnier, O. Chaix-Pluchery, C. Verrier, E. Appert, V. Consonni, Effects of Hexamethylenetetramine on the Nucleation and Radial Growth of ZnO Nanowires by Chemical Bath Deposition, J. Phys. Chem. C. 120 (2016) 5242–5250. doi:10.1021/acs.jpcc.6b00479.

[14] O. Marin, M. Tirado, N. Budini, E. Mosquera, C. Figueroa, D. Comedi, Photoluminescence from c-axis oriented ZnO films synthesized by sol-gel with diethanolamine as chelating agent, Mater. Sci. Semicond. Process. 56 (2016) 59–65. doi:10.1016/j.mssp.2016.07.007.

[15] L. Znaidi, Sol-gel-deposited ZnO thin films: A review, Mater. Sci. Eng. B Solid-State Mater. Adv. Technol. 174 (2010) 18–30. doi:10.1016/j.mseb.2010.07.001.

[16] O. Marin, G. Grinblat, A.M. Gennaro, M. Tirado, R.R. Koropecki, D. Comedi, On the origin of white photoluminescence from ZnO nanocones/porous silicon heterostructures at room temperature, Superlattices Microstruct. 79 (2015) 29–37. doi:10.1016/j.spmi.2014.12.016.

[17] K. Byrappa, T. Adschiri, Hydrothermal technology for nanotechnology, Prog. Cryst. Growth Charact. Mater. 53 (2007) 117–166. doi:10.1016/j.pcrysgrow.2007.04.001.

[18] S.P. Garcia, S. Semancik, Controlling the morphology of zinc oxide nanorods crystallized from aqueous solutions: The effect of crystal growth modifiers on aspect ratio, Chem. Mater. 19 (2007) 4016–4022. doi:10.1021/cm061977r.

[19] C.H. Lu, Y.C. Lai, R.B. Kale, Influence of alkaline sources on the structural and morphological properties of hydrothermally derived zinc oxide powders, J. Alloys Compd. 477 (2009) 523–528. doi:10.1016/j.jallcom.2008.10.076.

[20] D.A. Kitchaev, G. Ceder, Evaluating structure selection in the hydrothermal growth of FeS 2 pyrite and marcasite, Nat. Commun. 7 (2016) 1–7. doi:10.1038/ncomms13799.

[21] A. Navrotsky, Energetic clues to pathways to biomineralization: Precursors, clusters, and nanoparticles, Proc. Natl. Acad. Sci. 101 (2004) 12096–12101. doi:10.1073/pnas.0404778101.

[22] N. Asakuma, H. Hirashima, H. Imai, T. Fukui, M. Toki, Crystallization and Reduction of Sol-Gel-Derived Zinc Oxide Films by Irradiation with Ultraviolet Lamp, J. Sol-Gel Sci. Technol. 26 (2003) 181–184. doi:10.1023/A:102078251.

[23] N. Asakuma, H. Hirashima, H. Imai, T. Fukui, A. Maruta, M. Toki, K. Awazu, Photocrystallization of amorphous ZnO, J. Appl. Phys. 92 (2002) 5707–5710. doi:10.1063/1.1513197.

[24] O. Marin, A. María Gennaro, M. Tirado, R.R. Koropecki, D. Comedi, White light from annealed porous silicon: Broadband emission from violet to the near infrared, Mater. Lett. 150 (2015) 55–58. doi:10.1016/j.matlet.2015.03.003.

[25] P. Galář, B. Dzurňák, P. Malý, J. Čermák, A. Kromka, M. Omastová, B. Rezek, Chemical changes and photoluminescence properties of UV modified polypyrrole, Int. J. Electrochem. Sci. 8 (2013) 57–70.

[26] A. Stevanovic, M. Büttner, Z. Zhang, J.T. Yates, Photoluminescence of $TiO_2$: effect of UV light and adsorbed molecules on surface band structure., J. Am. Chem. Soc. 134 (2012) 324–32. doi:10.1021/ja2072737.

[27] M.A. Reshchikov, Y.T. Moon, X. Gu, B. Nemeth, J. Nause, H. Morkoç, Unstable luminescence in GaN and ZnO, Phys. B Condens. Matter. 376–377 (2006) 715–718. doi:10.1016/j.physb.2005.12.179.

[28] A. Šarić, G. Štefanić, G. Dražić, M. Gotić, Solvothermal synthesis of zinc oxide microspheres, J. Alloys Compd. 652 (2015) 91–99. doi:10.1016/j.jallcom.2015.08.200.

[29] R. Razali, A.K. Zak, W.H.A. Majid, M. Darroudi, Solvothermal synthesis of microsphere ZnO nanostructures in DEA media, Ceram. Int. 37 (2011) 3657–3663. doi:10.1016/j.ceramint.2011.06.026.

[30] H. Jiang, J. Hu, F. Gu, C. Li, Large-scaled, uniform, monodispersed ZnO

colloidal microspheres, J. Phys. Chem. C. 112 (2008) 12138–12141. doi:10.1021/jp8024232.

[31] M. Suryanarayana, C., Grant Norton, X-Ray Diffraction A practical Approach, Springer Science+Business Media New York, 1998. doi:10.1017/CBO9781107415324.004.

[32] C. Bouvy, W. Marine, R. Sporken, B.L. Su, Photoluminescence properties and quantum size effect of ZnO nanoparticles confined inside a faujasite X zeolite matrix, Chem. Phys. Lett. 428 (2006) 312–316. doi:10.1016/j.cplett.2006.06.106.

[33] N. Wang, Y. Yang, G. Yang, Great blue-shift of luminescence of ZnO nanoparticle array constructed from ZnO quantum dots, Nanoscale Res. Lett. 6 (2011) 2–7. doi:10.1186/1556-276X-6-338.

[34] B.D. Cullity, S.R. Stock, Elements of X-Ray Diffraction, Third Edit, Pearson Education Limited, 2014.

[35] A. Khorsand Zak, W.H. Abd. Majid, M.E. Abrishami, R. Yousefi, X-ray analysis of ZnO nanoparticles by Williamson-Hall and size-strain plot methods, Solid State Sci. 13 (2011) 251–256. doi:10.1016/j.solidstatesciences.2010.11.024.

[36] J. Rodríguez-Carvajal, Recent advances in magnetic structure determination by neutron powder diffraction, Phys. B Condens. Matter. 192 (1993) 55–69. doi:10.1016/0921-4526(93)90108-I.

[37] H. Karzel, W. Potzel, M. Köfferlein, W. Schiessl, M. Steiner, U. Hiller, G. Kalvius, D. Mitchell, T. Das, Lattice dynamics and hyperfine interactions in ZnO and ZnSe at high external pressures, Phys. Rev. B - Condens. Matter Mater. Phys. 53 (1996) 11425–11438. doi:10.1103/PhysRevB.53.11425.

[38] A. Shalimov, W. Paszkowicz, K. Grasza, P. Skupiński, A. Mycielski, J. Bak-Misiuk, X-ray characterisation of a bulk ZnO crystal, Phys. Status Solidi Basic Res. 244 (2007) 1573–1577. doi:10.1002/pssb.200675143.

[39] P. Hosseini Vajargah, H. Abdizadeh, R. Ebrahimifard, M.R. Golobostanfard, Sol–gel derived ZnO thin films: Effect of amino-additives, Appl. Surf. Sci. 285 (2013) 732–743. doi:10.1016/j.apsusc.2013.08.118.

[40] A. Šarić, I. Despotović, G. Štefanić, G. Dražić, The Influence of Ethanolamines on the Solvothermal Synthesis of Zinc Oxide: A Combined Experimental and Theoretical Study, ChemistrySelect. 2 (2017) 10038–10049. doi:10.1002/slct.201701692.

[41] R. Xie, T. Sekiguchi, T. Ishigaki, N. Ohashi, D. Li, R. Xie, Enhancement and

patterning of ultraviolet emission in ZnO with an electron beam Enhancement and patterning of ultraviolet emission in ZnO with an electron beam, Appl. Phys. Lett. 88 (2006) 134103. doi:10.1063/1.2189200.

[42] R. Xie, D. Li, D. Yang, Thermal-desorption induced enhancement and patterning of ultraviolet emission in chemically grown ZnO Thermal-desorption induced enhancement and patterning of ultraviolet emission in chemically grown ZnO, Nanotechnology. 17 (2006) 2789–2793. doi:10.1088/0957-4484/17/11/011.

[43] I.K. Akopyan, M.E. Labzovskaya, A.A. Lisachenko, B. V Novikov, A.Y. Serov, V. V Titov, N.G. Filosofov, Manifestation of Oxygen Desorption in Photoluminescence Spectra of ZnO, Phys. Solids State. 58 (2016) 1767–1771. doi:10.1134/S1063783416090031.

[44] C. Jin, A. Tiwari, R.J. Narayan, Ultraviolet-illumination-enhanced photoluminescence effect in zinc oxide thin films Ultraviolet-illumination-enhanced photoluminescence effect in zinc oxide, J. Appl. Phys. 98 (2005) 083707. doi:10.1063/1.2108156.

[45] F. Oba, M. Choi, I. Tanaka, Point defects in ZnO: an approach from first principles, Sci. Technol. Adv. Mater. 12 (2011) 034302. doi:10.1088/1468-6996/12/3/034302.